Chemical Science

ROYAL SOCIETY OF CHEMISTRY

EDGE ARTICLE

View Article Online
View Journal | View Issue

Check for updates

Cite this: *Chem. Sci.*, 2026, **17**, 2767

All publication charges for this article have been paid for by the Royal Society of Chemistry

Received 20th August 2025
Accepted 3rd December 2025

DOI: 10.1039/d5sc06382e

rsc.li/chemical-science

Open Access Article. Published on 04 December 2025. Downloaded on 4/6/2026 6:27:56 PM. This article is licensed under a Creative Commons Attribution-NonCommercial 3.0 Unported Licence.

# Spinel-type $Al_4C_3$ attainable above 7 GPa and more high-pressure phases of $Al_4C_3$

Mitchell Falgoust and Peter Kroll *

We predict that $Al_4C_3$ adopts a cubic, anti-spinel-type structure ($Al_4C_3$-II) between 7 and 33 GPa, peaking in stability relative to other $Al_4C_3$ structures at 26 GPa. At ambient pressure, $Al_4C_3$-II is mechanically robust, with a bulk modulus of 160 GPa and a Vickers hardness of around 30 GPa. Beyond $Al_4C_3$-II, we identify three additional post-spinel phases appearing in the $Al_4C_3$ phase diagram, including an anti-$Th_3P_4$-type at 140 GPa. The clear enthalpy differences under pressure leave little doubt that the known trigonal $R\bar{3}m$ ground state of $Al_4C_3$ will undergo multiple phase transitions. The accessible pressure window for spinel-type $Al_4C_3$-II is easily accessible in both laser-heated diamond anvil cell and large-volume multi-anvil cell experiments. We therefore encourage experimental exploration of the Al–C system at high pressure.

## Introduction

High-pressure chemistry is a rich field in materials research, and advanced synthesis techniques have delivered a variety of new compounds in recent times.[1–4] A notable research method is the laser heating-diamond anvil cell (LH-DAC) used in conjunction with *in situ* X-ray diffraction (XRD).[5–7] Modern LH-DAC equipment can explore temperatures and pressures above ~5000 K and 300 GPa,[8–10] and enables dynamic compression rates of several 100 GPa $s^{-1}$.[11–13] Larger volumes of material can be synthesized using Multi-Anvil-Cells (MAC) at pressures up to 50 GPa.[14]

Computational methods are now a standard tool for characterizing synthesized materials and are essential for exploring the phase space and advancing experimental research at high pressure.[15,16] For example, the spinel-type γ-$Si_3N_4$ was achieved at 15 GPa and 2000 K through a collaborative effort of computation and experiment.[17] Recently, after more than three decades of effort, a crystal phase of $C_3N_4$ was synthesized at high pressure (>100 GPa).[18–21]

Hitherto, the only known polymorph of $Al_4C_3$ is the trigonal ($R\bar{3}m$) ground state structure.[22–24] The high-pressure behavior of $Al_4C_3$ was explored up to 6 GPa at 300 K.[25] Exploration at higher temperatures occurred only up to 8 GPa, but resulted in an incongruent thermal decomposition of $Al_4C_3$.[26,27] Recently, $M_4C_3$ with anti-$Th_3P_4$ type structures have been synthesized for $Dy_4C_3$ at 19 GPa and for $Sc_4C_3$ at 10 GPa.[28,29] Despite its simplicity, $Al_4C_3$ appears to have been overlooked,[30,31] and our own efforts had been communicated but not published. However, its composition suggests it may display a similar rich high-pressure chemistry as $Si_3N_4$.[32–38]

## Results and discussion

While computing several hundred polymorphs with composition $A_4X_3$ at different pressures, we ultimately identified four high-pressure modifications of $Al_4C_3$, indexed with Roman numerals (II, III, IV, and V), that surpass the trigonal ground-state modification $Al_4C_3$-I. In sequence, these are an anti-spinel type, an anti-$CaFe_2O_4$-like orthorhombic modification, an anti-$CaFe_2O_4$-type, and an anti-$Th_3P_4$ type. Polyhedral structure depictions are shown in Fig. 1.

Ground state energies, lattice parameters, volumes, and bulk moduli of the structures are given in Table 1. The energy–volume, $\Delta E$–$V$, diagram is shown in Fig. 2a, the corresponding pressure–volume diagram in Fig. 2b, and the enthalpy–pressure, $\Delta H$–$p$, diagram is presented in Fig. 2c. Accordingly, the ground state modification will transform into the denser (anti-) spinel type of $Al_4C_3$-II at 7 GPa. This is a relatively low-pressure process that can be attained with various experimental equipment, including large-volume presses. The largest enthalpy difference of $Al_4C_3$-II to another phase, hence the maximum driving force for its formation, about 0.2 eV/$Al_4C_3$, is attained at 26 GPa. At 33 GPa, cubic $Al_4C_3$-II will be superseded by an orthorhombic structure that is related to the (anti-) $CaFe_2O_4$-type. This $Al_4C_3$-III remains favored up to 50 GPa, at which point it will transform into an

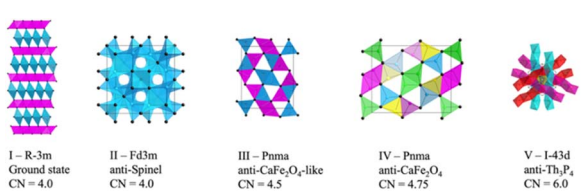


Fig. 1 The five phases of $Al_4C_3$ studied. Space groups and (average) coordination numbers (CN) of Al are indicated. Black spheres represent carbon; aluminum is depicted in colored polyhedra.

*Department of Chemistry and Biochemistry, The University of Texas at Arlington, 700 Planetarium Place, Arlington, Texas 76019, USA. E-mail: pkroll@uta.edu*

© 2026 The Author(s). Published by the Royal Society of Chemistry

Open Access Article. Published on 04 December 2025. Downloaded on 4/6/2026 6:27:56 PM. This article is licensed under a Creative Commons Attribution-NonCommercial 3.0 Unported Licence.

Table 1 Energy, lattice parameters, and volume of $Al_4C_3$ structures. The bulk modulus $B_0$ is computed from $E-V$ data using the Murnaghan equation of state

| | Energy (eV/$Al_4C_3$) | Lattice parameters (Å) | Volume (Å$^3$/$Al_4C_3$) | Bulk modulus (GPa) |
|---|---|---|---|---|
| I | −62.89 | $a = 3.33$<br>$c = 24.88$ | 79.64 | 172 |
| II | −62.81 | $a = 8.53$ | 77.65 | 176 |
| III | −61.83 | $a = 9.24$<br>$b = 3.12$<br>$c = 10.08$ | 72.56 | 170 |
| IV | −61.02 | $a = 8.79$<br>$b = 3.03$<br>$c = 10.45$ | 69.61 | 171 |
| V | −59.56 | $a = 6.48$ | 68.00 | — |

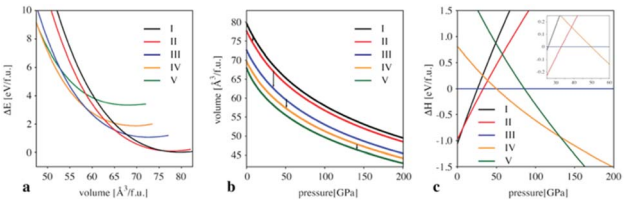


Fig. 2 (a) Energy–volume, $\Delta E-V$, diagram of relevant $Al_4C_3$ polymorphs. The energy is given relative to $Al_4C_3$-I. (b) Pressure–volume diagram of relevant $Al_4C_3$ polymorphs. The arrows indicate transition pressures between the phases. Note that $Al_4C_3$-V is mechanically unstable below 30 GPa. (c) Enthalpy–volume, $\Delta H-p$, diagram of relevant $Al_4C_3$ polymorphs. The enthalpy is given relative to $Al_4C_3$-III. The insert in the upper right corner details the transition sequence II–III–IV between 25 and 60 GPa. Black, red, blue, orange, and green lines represent $Al_4C_3$-I, II, III, IV, and V, respectively.

(anti-) $CaFe_2O_4$-type. Finally, at pressures above 140 GPa, an (anti-) $Th_3P_4$-type of $Al_4C_3$-V will be the most favorable structure. This final structure resembles the high-pressure phases of $Sc_4C_3$ and $Dy_4C_3$, attained at 10 and 19 GPa, respectively.[28,29] Hence, the larger trivalent cations of Sc and Dy attain the (anti-) $Th_3P_4$-type at much lower pressures than the smaller $Al^{3+}$ – a trend commonly observed in high-pressure chemistry of elements and compounds, including sesquioxides and sesquisulfide.[39–41] As expected, the densities of the $Al_4C_3$ polymorphs increase from phase I to V. Since the bulk moduli of the polymorphs are comparable, the initial slopes of the pressure–volume graphs (Fig. 2b) are very similar. That they remain so indicates a similar pressure dependence of the compressibility of the polymorphs. The average coordination number of $Al_4C_3$ polymorphs increases from phase I to V—except for the transition from the ground-state to the spinel-type structure (Fig. 1). This progression of phases thus reflects a systematic densification and coordination enhancement under pressure. The sequence of phase transformations, including transition pressure $p_t$ and volume change at $p_t$, is summarized by

$$\mathrm{I} \xrightarrow[-2.5\%]{7\ \mathrm{GPa}} \mathrm{II} \xrightarrow[-6.6\%]{33\ \mathrm{GPa}} \mathrm{III} \xrightarrow[-3.8\%]{50\ \mathrm{GPa}} \mathrm{IV} \xrightarrow[-3.0\%]{140\ \mathrm{GPa}} \mathrm{V}$$

At ambient pressure, the energy difference between the (anti-) spinel-type of $Al_4C_3$-II and the ground state modification $Al_4C_3$-I is only 80 meV/$Al_4C_3$. LDA calculations even place $Al_4C_3$-II below $Al_4C_3$-I by 23 meV/$Al_4C_3$, although both structures are built up by $AlC_4$-tetrahedra only, and, thus, the number of nearest atoms (coordination number) of Al is identical.

Table 2 Elastic constants (GPa) of $Al_4C_3$ polymorphs (I–V) computed at zero pressure (0 GPa)

| | I | II | III | IV | V |
|---|---|---|---|---|---|
| $C_{11}$ | 347 | 342 | 306 | 351 | 110 |
| $C_{22}$ | 347 | 342 | 424 | 510 | 110 |
| $C_{33}$ | 397 | 342 | 455 | 407 | 110 |
| $C_{44}$ | 111 | 168 | 17 | 65 | −966 |
| $C_{55}$ | 116 | 168 | 17 | 53 | −966 |
| $C_{66}$ | 116 | 168 | 151 | 141 | −966 |
| $C_{12}$ | 124 | 94 | 65 | 76 | 134 |
| $C_{13}$ | 55 | 94 | 78 | 44 | 134 |
| $C_{14}$ | 14 | 0 | 0 | 0 | 0 |
| $C_{23}$ | 55 | 94 | 47 | 44 | 134 |

The elastic constants of $Al_4C_3$ polymorphs (I–V) computed at zero pressure are shown in Table 2. Based on stability criteria,[42,43] the structures of $Al_4C_3$-I–IV are mechanically stable at ambient pressure. Thus, the high-pressure phases may be recoverable. While $Al_4C_3$-V is mechanically stable at 140 GPa, it becomes unstable below ∼30 GPa. A possible distortion along a Bain strain path may transform it into the spinel-type $Al_4C_3$-II.[33] The elastic constants can be used to compute the aggregate moduli, particularly the elastic shear modulus $G$. We obtain 123, 148, 70, and 110, for $Al_4C_3$-I–IV, respectively. Using the formula of Chen,[44] we estimate the Vickers hardness of $Al_4C_3$-I to 22 GPa and that of spinel-type $Al_4C_3$-II to 30 GPa. All polymorphs of $Al_4C_3$ presented here are semi-conductors, with band gaps of 1.6, 1.4, 1.9, 2.2, and 2.5 eV (GGA values) for $Al_4C_3$-I–V, respectively.

## Computational method

We started our search for potential high-pressure modifications of $Al_4C_3$ by screening models that we previously considered for $Si_3N_4$.[45] The results were confirmed by evolutionary algorithms using the USPEX code,[46–48] with a slight modification to $Al_4C_3$-III. All structures were computed using density functional theory (DFT), implemented with the Vienna *Ab initio*


© 2026 The Author(s). Published by the Royal Society of Chemistry

Open Access Article. Published on 04 December 2025. Downloaded on 4/6/2026 6:27:56 PM. This article is licensed under a Creative Commons Attribution-NonCommercial 3.0 Unported Licence.

Simulations Package (VASP).[49,50] We employed the projector augmented wave (PAW) formalism, along with the strongly constrained and approximately normed (SCAN) functional, for electron correlation and exchange.[51–53] A plane wave energy cutoff of 500 eV was applied, and fine grids sampled the Brillouin zone with spacings of 0.030–0.040 $Å^{-1}$.[54] With these parameters, forces, and energies converged to within 5 meV $Å^{-1}$ and 0.1 meV per atom, respectively. Throughout the work, we approximate Gibbs energy differences by enthalpy differences, hence $\Delta G \approx \Delta H$. Potential contributions from defects, non-stoichiometry, or surface effects during growth may be factors that alter the thermodynamic balance through configurational or vibrational entropy. We assume that if these effects occur, they affect all structures similarly. Remaining entropy differences are, in general, much smaller in comparison to the much larger variation of $\Delta H$ within a few GPa of pressure. Justification for this common approach stems from calculations of the phase boundary between the β- and γ-phase of $Si_3N_4$, with γ-$Si_3N_4$ adopting the spinel-structure,[55] and from the prediction of a synthesis of $Hf_3N_4$ with $Th_3P_4$-structure from the elements.[56]

## Conclusions

We predict a cubic (anti-) spinel-type of $Al_4C_3$ succeeding the known trigonal ground state modification at higher pressures. While $Al_4C_3$-II is 0.08 meV/$Al_4C_3$ above the ground state at ambient pressure, it becomes thermodynamically favored between 7 and 33 GPa with a maximum enthalpy difference (hence, driving force) of 0.2 eV $f.u.^{-1}$ at 26 GPa. $Al_4C_3$-II is also stable against decomposition into the elements, by 1.8 and 1.7 eV/$Al_4C_3$ at ambient pressure and 30 GPa, respectively. The reported energy differences are well above the "uncertainty" of DFT calculations for enthalpies of formation differences, about 10 meV per atom.[57] The proposed stability range of spinel-type $Al_4C_3$ is accessible with large-volume presses[58] or LH-DAC.[5] However, high temperatures may be required to facilitate the transition. Previous experiments examined pressures up to 8 GPa and maintained temperatures below 2500 K.[26,27] $Al_4C_3$-II is mechanically stable at ambient pressure, with a bulk modulus of 160 GPa comparable to that of $Fe_3C$ or ThC.[59,60] The hardness of $Al_4C_3$-II will be substantially higher than that of the known modification, we estimate $H_v \approx 30$ GPa for $Al_4C_3$-II.

Beyond $Al_4C_3$-II, the phase diagram of $Al_4C_3$ features three post-spinel modifications. Several other materials also exhibit post-spinel modifications, including $CaFe_2O_4$, $ZnGa_2O_4$, and $CdCr_2Se_4$.[61–66] For $Si_3N_4$, such phases were also proposed,[45,61] but ultimately a pernitride $SiN_2$ with $N_2^{4-}$-units emerged. Motivated by this analogy, we explored a series of Al–C compounds with $C_2$-dimers in various oxidation states ($C_2^{2-}$, $C_2^{4-}$, and $C_2^{6-}$), but none yielded a thermodynamically stable polymorph. In addition to $Al_4C_3$-I to $Al_4C_3$-V, we also identified several candidate structures of $Al_4C_3$ that, at certain pressures, approach the stability of the thermodynamically most favorable structure shown here. These include types related to $SrPb_2O_4$, $P_4S_3$, and further variants of the $CaFe_2O_4$-type. While our calculations neglect possible contributions from defects, non-stoichiometry, or surface effects – factors that could alter the thermodynamic balance through configurational or vibrational entropy – it is evident that $Al_4C_3$ will undergo pressure-induced phase transitions. We therefore encourage experimental efforts to synthesize the predicted $Al_4C_3$-II modification and advance the high-pressure chemistry of metal carbides.

## Author contributions

Mitchell Falgoust: writing – review & editing, writing – original draft, visualization, methodology, investigation, formal analysis, data curation. Peter Kroll: writing – review & editing, writing – original draft, visualization, supervision, resources, project administration, methodology, investigation, funding acquisition, formal analysis, data curation, conceptualization.

## Conflicts of interest

There are no conflicts to declare.

## Data availability

The data supporting the article is available from the corresponding author upon reasonable request.

## Acknowledgements

This work used Stampede3 at Texas Advanced Computing Center (TACC) through allocation DMR190103 from the Advanced Cyberinfrastructure Coordination Ecosystem: Services & Support (ACCESS) program, which is supported by National Science Foundation grants #2138259, #2138286, #2138307, #2137603, and #2138296. Additional computational work was made possible by the High-Performance Computing facilities at the University of Texas at Arlington. MF was supported through a Graduate Dean Research Assistance fellowship.

## References

1 J. V. Badding, High-Pressure Synthesis, Characterization, and Tuning of Solid State Materials, *Annu. Rev. Mater. Res.*, 1998, **28**, 631–658.
2 Y. Fei and M. J. Walter, *Static and Dynamic High Pressure Mineral Physics*, Cambridge University Press, Cambridge, 2022.
3 W. Zhao, J. Zhang, Z. Sun, G. Xiao, H. Zheng, K. Li, M.-R. Li and B. Zou, Chemical Synthesis Driven by High Pressure, *CCS Chem.*, 2025, **7**, 1250–1271.
4 S. Guo, Y. Zhang, K. Bu, Y. Zhan and X. Lü, High-Pressure Chemistry of Functional Materials, *Chem. Commun.*, 2025, **61**, 1773–1789.
5 A. Jayaraman, Diamond Anvil Cell and High-Pressure Physical Investigations, *Rev. Mod. Phys.*, 1983, **55**, 65.
6 W. A. Bassett, Diamond Anvil Cell, 50th Birthday, *High Pressure Res.*, 2009, **29**, Cp5–Cp186.
7 M. E. Alabdulkarim, W. D. Maxwell, V. Thapliyal and J. L. Maxwell, A Comprehensive Review of High-Pressure

Open Access Article. Published on 04 December 2025. Downloaded on 4/6/2026 6:27:56 PM. This article is licensed under a Creative Commons Attribution-NonCommercial 3.0 Unported Licence.

Laser-Induced Materials Processing, Part I: Laser-Heated Diamond Anvil Cells, *J. Manuf. Mater. Process.*, 2022, **6**, 111.
8 L. R. Benedetti and P. Loubeyre, Temperature Gradients, Wavelength-Dependent Emissivity, and Accuracy of High and Very-High Temperatures Measured in the Laser-Heated Diamond Cell, *High Pressure Res.*, 2004, **24**, 423–445.
9 S. Tateno, K. Hirose, Y. Ohishi and Y. Tatsumi, The Structure of Iron in Earth's Inner Core, *Science*, 2010, **330**, 359–361.
10 N. Dubrovinskaia, *et al.*, Terapascal Static Pressure Generation with Ultrahigh Yield Strength Nanodiamond, *Sci. Adv.*, 2016, **2**, e1600341.
11 M. Ricks, A. E. Gleason, F. Miozzi, H. Yang, S. Chariton, V. B. Prakapenka, S. Sinogeikin, R. L. Sandberg, W. L. Mao and S. Pandolfi, Phase Transition Kinetics Revealed by in Situ X-Ray Diffraction in Laser-Heated Dynamic Diamond Anvil Cells, *Phys. Rev. Res.*, 2024, **6**, DOI: 10.1103/PhysRevResearch.6.0133316.
12 L. Q. Huston, L. Miyagi, R. J. Husband, K. Glazyrin, C. Kiessner, M. Wendt, H. P. Liermann and B. T. Sturtevant, New Dynamic Diamond Anvil Cell for Time-Resolved Radial X-Ray Diffraction, *Rev. Sci. Instrum.*, 2024, **95**, 043904.
13 W. J. Evans, C. S. Yoo, G. W. Lee, H. Cynn, M. J. Lipp and K. Visbeck, Dynamic Diamond Anvil Cell (Ddac): A Novel Device for Studying the Dynamic-Pressure Properties of Materials, *Rev. Sci. Instrum.*, 2007, **78**, 073904.
14 J.-a. Xu and H.-k. Mao, Moissanite: A Window for High-Pressure Experiments, *Science*, 2000, **290**, 783–785.
15 N. P. Salke, *et al.*, Prediction and Synthesis of Dysprosium Hydride Phases at High Pressure, *Inorg. Chem.*, 2020, **59**, 5303–5312.
16 P. V. Marshall, S. D. Thiel, E. E. Cote, R. Hrubiak, M. L. Whitaker, Y. Meng and J. P. S. Walsh, Combined First-Principles and Experimental Investigation into the Reactivity of Codeposited Chromium-Carbon under Pressure, *ACS Mater. Au*, 2024, **4**, 393–402.
17 A. Zerr, G. Miehe, G. Serghiou, M. Schwarz, E. Kroke, R. Riedel, H. Fuess, P. Kroll and R. Boehler, Synthesis of Cubic Silicon Nitride, *Nature*, 1999, **400**, 340–342.
18 A. Y. Liu and M. L. Cohen, Prediction of New Low Compressibility Solids, *Science*, 1989, **245**, 841–842.
19 P. V. Zinin, L. C. Ming, S. K. Sharma, S. M. Hong, Y. Xie, T. Irifune and T. Shinmei, Synthesis of New Cubic $C_3N_4$ and Diamond-Like $BC_3$ Phases under High Pressure and High Temperature, in *Joint 21st AIRAPT and 45th EHPRG International Conference on High Pressure Science and Technology*, 2008, vol. 121.
20 D. Laniel, *et al.*, Synthesis of Ultra-Incompressible and Recoverable Carbon Nitrides Featuring $CN_4$ Tetrahedra, *Adv. Mater.*, 2024, **36**, 2308030.
21 D. Laniel, *et al.*, High-Pressure Synthesis of Op28-$C_3N_4$ Recoverable to Ambient Conditions, *Adv. Funct. Mater.*, 2025, **35**, 2416892.
22 M. von Stackelberg and E. Schorrenberg, The Structure of Aluminium Carbide $Al_4C_3$, *Z. Phys. Chem. B*, 1934, **27**, 37.
23 J. H. Cox and L. M. Pidgeon, The X-Ray Diffraction Patterns of Aluminum Carbide $Al_4C_3$ and Aluminum Oxycarbide $Al_4O_4C$, *Can. J. Chem.*, 1963, **41**, 1414–1416.
24 T. M. Gesing and W. Jeitschko, The Crystal Structure and Chemical Properties of $U_2Al_3C_4$ and Structure Refinement of $Al_4C_3$, *Z. Naturforsch., B: J. Chem. Sci.*, 1995, **50**, 196–200.
25 V. L. Solozhenko and O. O. Kurakevych, Equation of State of Aluminum Carbide $Al_4C_3$, *Solid State Commun.*, 2005, **133**, 385–388.
26 J. C. Schuster, A Reinvestigation of the Thermal Decomposition of Aluminum Carbide and the Constitution of the Al-C System, *J. Phase Equilib.*, 1991, **12**, 546–549.
27 V. Turkevich, A. Garan, O. Kulik and I. Petrusha, Phase Diagram and Diamond Synthesis in the Aluminum–Carbon System at a Pressure of 8 GPa, *Innovative Superhard Materials and Sustainable Coatings for Advanced Manufacturing*, 2005, pp. 335–343.
28 E. A. Juarez-Arellano, *et al.*, Formation of Scandium Carbides and Scandium Oxycarbide from the Elements at High-(P, T) Conditions, *J. Solid State Chem.*, 2010, **183**, 975–983.
29 F. I. Akbar, *et al.*, High-Pressure Synthesis of Dysprosium Carbides, *Front. Chem.*, 2023, **11**, DOI: 10.3389/fchem.2023.1210081.
30 L. Sun, Y. Gao, K. Yoshida, T. Yano and W. Wang, Prediction on Structural, Mechanical and Thermal Properties of $Al_4SiC_4$, $Al_4C_3$ and 4H-SiC under High Pressure by First-Principles Calculation, *Mod. Phys. Lett. B*, 2017, **31**, 1750080.
31 A. Pisch, A. Pasturel, G. Deffrennes, O. Dezellus, P. Benigni and G. Mikaelian, Investigation of the Thermodynamic Properties of $Al_4C_3$: A Combined DFT and DSC Study, *Comput. Mater. Sci.*, 2020, **171**, 109100.
32 E. Kroke, High-Pressure Syntheses of Novel Binary Nitrogen Compounds of Main Group Elements, *Angew. Chem., Int. Ed.*, 2002, **41**, 77–82.
33 P. Kroll, Pathways to Metastable Nitride Structures, *J. Solid State Chem.*, 2003, **176**, 530–537.
34 P. Kroll and M. Milko, Theoretical Investigation of the Solid State Reaction of Silicon Nitride and Silicon Dioxide Forming Silicon Oxynitride ($Si_2N_2O$) under Pressure, *Z. Anorg. Allg. Chem.*, 2003, **629**, 1737–1750.
35 E. Horvath-Bordon, R. Riedel, A. Zerr, P. F. McMillan, G. Auffermann, Y. Prots, W. Bronger, R. Kniep and P. Kroll, High-Pressure Chemistry of Nitride-Based Materials, *Chem. Soc. Rev.*, 2006, **35**, 987–1014.
36 B. H. Yu and D. Chen, Phase Transition Characters and Thermodynamics Modeling of the Newly-Discovered Wii- and Post-Spinel $Si_3N_4$ Polymorphs: A First-Principles Investigation, *Acta Metall. Sin. (Engl. Lett.)*, 2013, **26**, 131–136.
37 L. Cui, M. Hu, Q. Q. Wang, B. Xu, D. L. Yu, Z. Y. Liu and J. L. He, Prediction of Novel Hard Phases of $Si_3N_4$: First-Principles Calculations, *J. Solid State Chem.*, 2015, **228**, 20–26.
38 Q. H. Wu, Z. T. Huo, C. Chen, X. Q. Li, Z. Wang, C. J. Wang, L. J. Zhang, Y. F. Gao, M. Xiong and K. M. Pan, Prediction of Four $Si_3N_4$ Compounds by First-Principles Calculations, *AIP Adv.*, 2023, **13**, DOI: 10.1063/5.0130194.


© 2026 The Author(s). Published by the Royal Society of Chemistry

Open Access Article. Published on 04 December 2025. Downloaded on 4/6/2026 6:27:56 PM. This article is licensed under a Creative Commons Attribution-NonCommercial 3.0 Unported Licence.

39 A. Mujica, A. Rubio, A. Muñoz and R. J. Needs, High-Pressure Phases of Group-IV, III–V, and II–VI Compounds, *Rev. Mod. Phys.*, 2003, **75**, 863–912.
40 L. Liu and W. A. Bassett, *Elements, Oxides, Silicates: High Pressure Phases with Implications for the Earth's Interior*, Oxford University Press, New York, 1986, p. 250.
41 F. J. Manjón and D. Errandonea, Pressure-Induced Structural Phase Transitions in Materials and Earth Sciences, *Phys. Status Solidi B*, 2009, **246**, 9–31.
42 J. F. Nye, *Physical Properties of Crystals: Their Representation by Tensors and Matrices*, Oxford University Press, 1985.
43 F. Mouhat and F.-X. Coudert, Necessary and Sufficient Elastic Stability Conditions in Various Crystal Systems, *Phys. Rev. B: Condens. Matter Mater. Phys.*, 2014, **90**, 224104.
44 X.-Q. Chen, H. Niu, D. Li and Y. Li, Modeling Hardness of Polycrystalline Materials and Bulk Metallic Glasses, *Intermetallics*, 2011, **19**, 1275–1281.
45 P. Kroll and J. von Appen, Post-Spinel Phases of Silicon Nitride, *Phys. Status Solidi B*, 2001, **226**, R6–R7.
46 A. R. Oganov and C. W. Glass, Crystal Structure Prediction Using Ab Initio Evolutionary Techniques: Principles and Applications, *J. Chem. Phys.*, 2006, **124**, 244704.
47 A. R. Oganov, A. O. Lyakhov and M. Valle, How Evolutionary Crystal Structure Prediction Works—and Why, *Acc. Chem. Res.*, 2011, **44**, 227–237.
48 A. O. Lyakhov, A. R. Oganov, H. T. Stokes and Q. Zhu, New Developments in Evolutionary Structure Prediction Algorithm USPEX, *Comput. Phys. Commun.*, 2013, **184**, 1172–1182.
49 P. Hohenberg and W. Kohn, Inhomogeneous Electron Gas, *Phys. Rev.*, 1964, **136**, B864–B871.
50 W. Kohn and L. J. Sham, Self-Consistent Equations Including Exchange and Correlation Effects, *Phys. Rev.*, 1965, **140**, A1133–A1138.
51 G. Kresse and J. Furthmüller, Efficient Iterative Schemes for Ab Initio Total-Energy Calculations Using a Plane-Wave Basis Set, *Phys. Rev. B: Condens. Matter Mater. Phys.*, 1996, **54**, 11169–11186.
52 G. Kresse and D. Joubert, From Ultrasoft Pseudopotentials to the Projector Augmented-Wave Method, *Phys. Rev. B: Condens. Matter Mater. Phys.*, 1999, **59**, 1758–1775.
53 J. Sun, A. Ruzsinszky and J. P. Perdew, Strongly Constrained and Appropriately Normed Semilocal Density Functional, *Phys. Rev. Lett.*, 2015, **115**, 036402.
54 H. J. Monkhorst and J. D. Pack, Special Points for Brillouin-Zone Integrations, *Phys. Rev. B*, 1976, **13**, 5188–5192.
55 A. Togo and P. Kroll, First-Principles Lattice Dynamics Calculations of the Phase Boundary between β-$Si_3N_4$ and γ-$Si_3N_4$ at Elevated Temperatures and Pressures, *J. Comput. Chem.*, 2008, **29**, 2255–2259.
56 P. Kroll, Hafnium Nitride with Thorium Phosphide Structure: Physical Properties and an Assessment of the Hf-N, Zr-N, and Ti-N Phase Diagrams at High Pressures and Temperatures, *Phys. Rev. Lett.*, 2003, **90**, 125501.
57 A. Wang, R. Kingsbury, M. McDermott, M. Horton, A. Jain, S. P. Ong, S. Dwaraknath and K. A. Persson, A Framework for Quantifying Uncertainty in DFT Energy Corrections, *Sci. Rep.*, 2021, **11**, 15496.
58 L. G. Khvostantsev and V. N. Slesarev, Large-Volume High-Pressure Devices for Physical Investigations, *Phys.-Usp.*, 2008, **51**, 1099–1104.
59 M. Umemoto and H. Ohtsuka, Mechanical Properties of Cementite, *ISIJ Int.*, 2022, **62**, 1313–1333.
60 C. Yu, *et al.*, Structural Phase Transition of ThC under High Pressure, *Sci. Rep.*, 2017, **7**, 96.
61 A. Zerr, A New High-Pressure Delta-Phase of $Si_3N_4$, *Phys. Status Solidi B*, 2001, **227**, R4–R6.
62 W. Xu, G. Hearne, S. Layek, D. Levy, M. Pasternak, G. K. Rozenberg and E. Greenberg, Interplay between Structural and Magnetic-Electronic Responses of $FeAl_2O_4$ to a Megabar: Site Inversion and Spin Crossover, *Phys. Rev. B*, 2018, **97**, 085120.
63 M. Sahu, Pressure-induced volume collapse and metallization in inverse spinel $Co_2TiO_4$, *J. Phys.: Condens. Matter.*, 2025, **37**, 345402.
64 I. Efthimiopoulos, Z. T. Y. Liu, M. Kucway, S. V. Khare, P. Sarin, V. Tsurkan, A. Loidl and Y. Wang, Pressure-Induced Phase Transitions in the $CdCr_2Se_4$ Spinel, *Phys. Rev. B*, 2016, **94**, 174106.
65 D. Errandonea, R. S. Kumar, Y. Ma and C. Y. Tu, High-Pressure Structural Stability of Spinel-Type $ZnGa_2O_4$: A Synchrotron X-Ray Diffraction Study, *Phys. Rev. B: Condens. Matter Mater. Phys.*, 2009, **79**, 024103.
66 T. Yamanaka, A. Uchida and Y. Nakamoto, Structural Transition of Post-Spinel Phases $CaMn_2O_4$, $CaFe_2O_4$, and $CaTi_2O_4$ under High Pressures up to 80 GPa, *Am. Mineral.*, 2008, **93**, 1874–1881.

© 2026 The Author(s). Published by the Royal Society of Chemistry